Additive Manufacturing Letters 7 (2023) 100162

Contents lists available at ScienceDirect

Additive Manufacturing Letters

journal homepage: www.elsevier.com/locate/addlet

Short Communication

Stability of vacancies in β-type Ti-15Mo-5Zr-3Al alloy fabricated via laser powder bed fusion

Masataka Mizuno[a,*], Kazuki Sugita[a], Kousuke Do[a], Takuya Ishimoto[a,b,c], Takayoshi Nakano[a,b], Hideki Araki[a]

[a] Division of Materials and Manufacturing Science, Graduate School of Engineering, Osaka University, 2-1 Yamadaoka, Suita, Osaka 565-0871, Japan
[b] Anisotropic Design and Additive Manufacturing Research Center, Osaka University, 2-1, Yamadaoka, Suita, Osaka 565-0871, Japan
[c] Aluminium Research Center, University of Toyama, 3190, Gofuku, Toyama 930-8555, Japan

ARTICLE INFO

Keywords:
Ti alloys
Laser powder bed fusion
First-principles calculation
Vacancy formation energy
Migration energy
Diffusion

ABSTRACT

The structural instability in the β-type titanium alloys could affect the stability of vacancies. The stability of vacancies in a β-type Ti-15Mo-5Zr-3Al alloy, fabricated via laser powder bed fusion (LPBF), was investigated using positron annihilation spectroscopy and first-principles calculations. The observed positron lifetimes were close to the experimental and calculated bulk lifetime of Ti-15Mo-5Zr-3Al, which indicates that vacancies were not detected in Ti-15Mo-5Zr-3Al by positron lifetime measurements. Therefore, for the first time, it has been confirmed that quenched-in vacancies are not introduced in the LPBF-manufactured β-type Ti-15Mo-5Zr-3Al despite the fast cooling rate in LPBF process. This feature is preferable for the structural stability in biomedical and industrial applications. The calculated atomic displacement from the ideal bcc lattice positions decreased in β-type Ti-Mo alloys with increasing Mo concentration, indicating that the bcc structure was stabilized by the added Mo. The calculated vacancy formation energies of Ti atoms in β-type Ti-14.5Mo and Ti-27.0Mo alloys exhibited an increasing trend with an increasing number of neighboring Mo atoms. Mo atoms also increased the migration energies of the neighboring paths of vacancies. The calculated results for Ti-15Mo-5Zr-3Al suggest that, while the bcc structure was stabilized by the Mo atoms in Ti-15Mo-5Zr-3Al, the migration and formation energies were still low enough for the diffusion of vacancies.

1. Introduction

β-type titanium alloys have attracted considerable attention as biomedical implant materials [1–4]. β-type Ti-15Mo-5Zr-3Al (wt%) is one of the most promising candidates for biomedical implant materials because of its low Young's modulus [5–7]. The control and stability of crystallographic texture of β-type Ti-15Mo-5Zr-3Al alloys, fabricated via laser powder bed fusion (LPBF) technologies, have been investigated [8–11]. The existence of quenched-in vacancies can be expected in LPBF-manufactured β-type Ti-15Mo-5Zr-3Al because of the fast cooling rate in the additive manufacturing process [12]. The cooling rate in LPBF process has been estimated to be 10^5 –10^7 K/s [13,14]. However, the anomalous fast diffusion, originating from the body-centered cubic (bcc) structure in the group-IVb β phase [15], could promote the annihilation of quenched-in vacancies. It has been reported that in β-type Ti, the elementary diffusion jump is a jump into a nearest-neighbor vacancy [16]. Therefore, the stability of these vacancies plays a key role in the diffusivity of β-type Ti. The bcc structure of β-type titanium alloys is stabilized by β-stabilizing elements [3] into them. In β-type Ti-15Mo-5Zr-3Al, the bcc structure is stabilized by Mo atoms. However, the effect of Mo atoms on the stability of the vacancies has not been experimentally or theoretically examined.

β-type Ti-Mo alloys have recently attracted considerable attention for theoretical studies [17–25]. Zhu et al. [20] investigated the variant selection in the $\beta \rightarrow \omega$ transformation of Ti-Mo alloy using virtual crystal approximation (VCA) [26,27]. Chen et al. [25] also investigated the role played by ω phase in the twining in Ti-Mo alloy using VCA. Cao et al. [19] systematically investigated the effect of Mo on the phase stability and elastic mechanical properties of β-type Ti-Mo alloys using coherent potential approximation (CPA) [28,29]. The instability of the bcc structure originated from harmonic phonon instabilities [30], which led to atomic displacement from the ideal bcc lattice positions. In the case of calculations for defect properties, structural relaxation around the defects or compositional fluctuation of neighboring atoms, which are not directly considered in the VCA and CPA methods, have a significant influence on the calculated results. These effects can be included in first-principles calculations, using the special quasirandom structure (SQS) method [31]. The SQS method has been applied to calculate the

* Corresponding author.
E-mail address: mizuno@mat.eng.osaka-u.ac.jp (M. Mizuno).

https://doi.org/10.1016/j.addlet.2023.100162
Received 17 May 2023; Received in revised form 18 June 2023; Accepted 10 July 2023

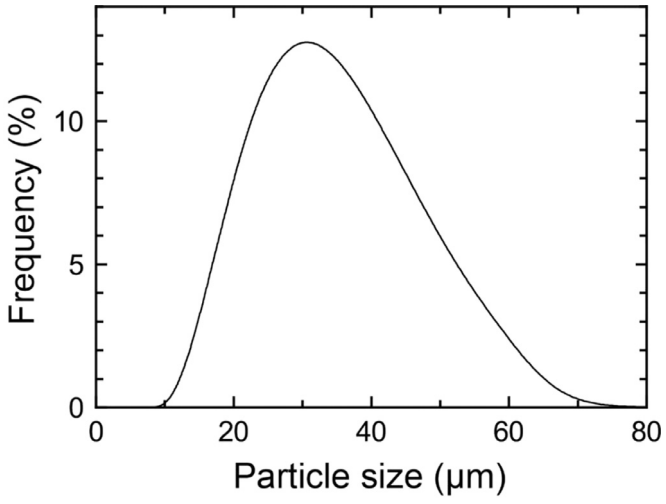

Fig. 1. Particle size distribution of the obtained powder of Ti-15Mo-5Zr-3Al.

structural and electric properties [17], as well as the phase diagram of Ti-Mo alloys [18]. However, the atomic displacement and defect properties of β-type Ti-Mo alloys have not been studied.

In this study, positron lifetime spectroscopy, which allows for the sensitive detection of vacancies on the order of ppm, was employed to identify lattice defects formed in an LPBF-manufactured β-type Ti-15Mo-5Zr-3Al. In addition, to quantitatively evaluate the formation and migration energies of vacancies in β-type Ti-Mo alloys and Ti-15Mo-5Zr-3Al, first-principles calculations were performed in combination with the SQS method. Our results highlight the importance of the stability of vacancies that affects the formation of lattice defects in the LPBF process.

2. Experimental and computational method

The starting material was an ingot with a nominal composition of Ti–15Mo–5Zr–3Al (wt%). The powder for the LPBF fabrication was developed by Ar gas atomization, which used an induction coil to melt the ingot (Osaka Titanium Technologies, Japan). The obtained powder was spherical particle, with a median particle size of 31.6 μm. The result of particle size distribution analysis is shown in Fig. 1. Rectangular samples with bottom dimensions of 5 mm × 5 mm were manufactured using an LPBF apparatus (EOS M290, EOS, Germany), equipped with a Yb fiber laser. To evaluate the effects of fabrication parameters on positron lifetime, the laser power and scanning speed were varied over a wide range and set to three conditions: 75 W and 250 mm/s, 300 W and 1000 mm/s, and 360 W and 1200 mm/s where a volumetric energy density of the laser was kept constant as 50 J/mm^3. This volumetric energy density was determined according to the literature [11] to obtain products with high density and smooth surface. Details of the process and the crystallographic textures of the fabricated products were reported by Ishimoto et al. [9,10]. To obtain the bulk positron lifetime of Ti–15Mo–5Zr–3Al, solution-treated samples cut from the ingot (Kobe Steel Ltd., Japan) were prepared by quenching in water at 1108 K after holding for 1h. Although, for this purpose, furnace cooling is preferable to avoid the formation of quenched-in vacancies, quenching in water was employed to maintain the β phase.

Positron lifetime measurements were performed using a digital oscilloscope (Lecroy WaveRunner 62-Xi) system, which yields a time resolution of 187 ps combined with photomultiplier tubes, mounted with BaF_2 scintillators. The positron lifetime spectra were obtained at a coincidence count rate of 120 counts per second and a total number of 10^5–10^6 coincidence counts. Resulting positron lifetime spectra were analyzed using the Resolution [32] and Positronfit Extended [33] programs. To identify the experimental positron lifetime, the positron bulk lifetime in Ti-15Mo-5Zr-3Al was calculated using the ABINIT code [34]. For the electron-positron correlation functional and enhancement factor, the functional parameterized by Boronski and Nieminen was used [35].

To evaluate the stability of vacancies, vacancy formation energies were obtained for β-type Ti-Mo alloys and Ti-15Mo-5Zr-3Al using first-principles calculations. the Vienna Ab initio Simulation Package (VASP) [36,37] was employed along with the generalized gradient approximation of Perdew–Burke–Ernzerhof (PBE) [38]. The potentials used were based on the projector augmented wave (PAW) method [39,40]. Disordered atomic arrangements were constructed using the SQS approach, with a supercell having 128 lattice sites in the bcc structure (4×4×4 unit cell). In this study, the atomic configurations were determined in the alloy so that the Warren–Cowley parameter [41] was close to zero up to the seventh nearest-neighbor shell. Twelve binary SQS models were constructed for β-type Ti-Mo alloys, ranging from 0.0625 to 0.90625 atomic fractions. To construct the SQS model of β-type Ti-15Mo-5Zr-3Al (Ti-8.10 at%Mo-2.84 at%Zr-5.76 at%Al), a supercell composed of 106 Ti, 10 Mo, 4 Zr and 8 Al atoms was employed. The composition of the supercell is Ti-7.81 at%Mo-3.12 at%Zr-6.25 at%Al. A kinetic-energy cutoff of 350 eV and a 4×4×4 k mesh was used in the Monkhorst–Pack scheme. The structural relaxation of the atoms was continued until the forces on all atoms were less than 0.02 eV/Å.

The vacancy formation energies of all sites in the supercell were calculated to evaluate the influence of Mo atoms on the vacancy formation energy. For a binary alloy, *AB*, the vacancy formation energy at site *A*, E_A^{Vac}, can be obtained as follows:

$$E_A^{Vac} = E_{tot}(n_A - 1, n_B) - E_{tot}(n_A, n_B) + \mu_A, \quad (1)$$

where E_{tot} is the total energy, n_A and n_B are the number of atoms of element *A* and *B*, respectively. The first and second terms in the right-hand side of Eq. (1) denote the total energy of the supercell including a vacancy of *A* atom and that of the defect-free supercell, respectively. μ_A is the chemical potential of element *A*. Finally, the chemical potentials of Ti and Mo atoms in the β-type Ti-Mo alloys were obtained using the value of the change in energy with the increasing Mo concentration. To obtain the chemical potentials of each element in the β-type Ti-15Mo-5Zr-3Al, six SQS models with the compositions slightly deviating from Ti-15Mo-5Zr-3Al was constructed. The chemical potentials of each element were determined using a linear regression analysis for the total energies of seven compositions including Ti-15Mo-5Zr-3Al.

3. Results and discussion

3.1. Positron lifetime of Ti-15Mo-5Zr-3Al

Fig. 2 shows one-component positron lifetime of Ti-15Mo-5Zr-3Al as a function of the scanning speed. Irrespective of the scanning speed, the positron lifetimes showed values in the range of 144–147 ps. The experimental and calculated bulk lifetimes of Ti-15Mo-5Zr-3Al are 144 and 143 ps, respectively. If quenched-in vacancies are introduced, the one-component positron lifetime significantly increases from the bulk lifetime because the ratios of the positron lifetimes between metal vacancies and perfect bulk lattices are more than 1.4 [42]. The difference between the observed positron lifetimes and the bulk lifetime in Ti-15Mo-5Zr-3Al were less than 4 ps, which indicates that the vacancy concentration was less than the order of ppm in the LPBF-manufactured Ti-15Mo-5Zr-3Al.

3.2. Atomic displacement in Ti-Mo alloy and Ti-15Mo-5Zr-3Al

Fig. 3 shows the mean atomic displacements from the ideal bcc lattice positions in the β-type Ti-Mo alloys and Ti-15Mo-5Zr-3Al. The displacement magnitudes decreased with increasing Mo concentration in the Ti-Mo alloys. The Ti and Mo atoms in Ti-15Mo-5Zr-3Al exhibited approximately the same displacement magnitude as the Ti and Mo atoms

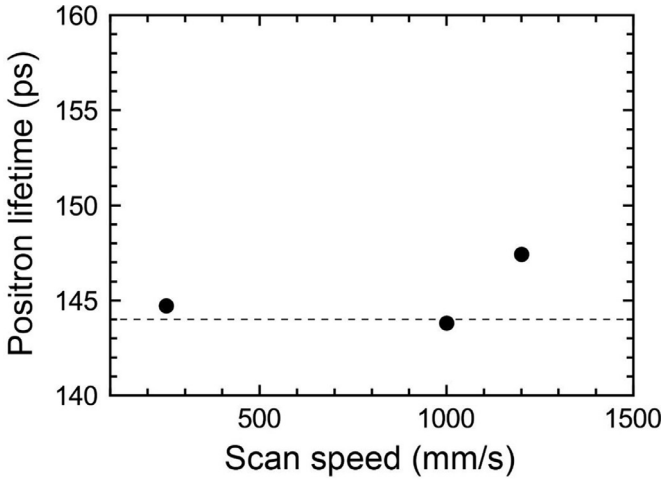

Fig. 2. One-component positron lifetime in Ti-15Mo-5Zr-3Al as a function of scanning speed. The experimental bulk lifetime is denoted by the broken line.

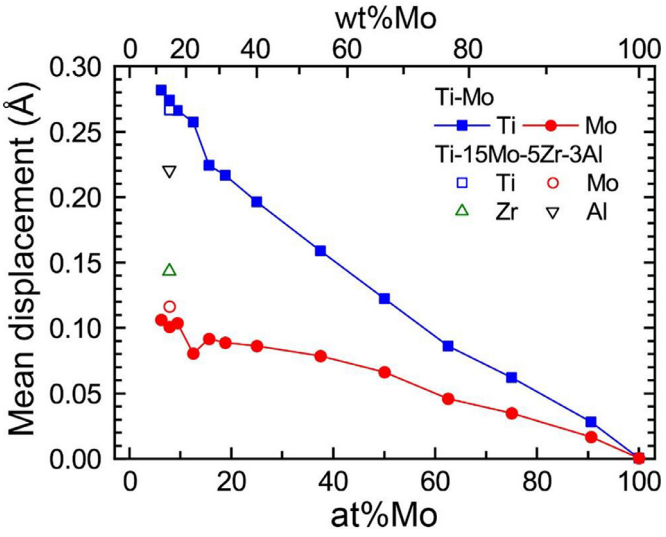

Fig. 3. Mean atomic displacement from the ideal bcc lattice positions in β-type Ti-Mo alloys and Ti-15Mo-5Zr-3Al.

in Ti-14.5Mo (7.8 at% Mo). In general, the atomic displacement from ideal lattice positions in solid solutions increases with the number of solute atoms. The opposite trend observed for β-type Ti-Mo alloys originated from the instability of the bcc structure of Ti [30]. Therefore, the Ti atoms exhibited approximately twice the mean atomic displacement, compared to that of the Mo atoms. Fig. 4 shows the atomic arrangement of Ti-14.5Mo (7.8 at% Mo), Ti-27.0Mo (15.6 at% Mo), and Ti-40.0Mo (25.0 at% Mo). The Ti and Mo atoms were randomly displaced from the ideal bcc lattice, and the amount of displacement was observed to decrease with increasing Mo concentration. These results indicate that the bcc structure was stabilized by the added Mo atoms. However, the displace magnitude in Ti-14.5Mo is still larger compared to that in the Mo-rich region, which is one of the possible causes of the lattice distortion observed in the LPBF-manufactured β-type Ti-15Mo-5Zr-3Al [43].

3.3. Density of states in Ti-Mo alloy

As shown in Figs. 3 and 4, the atomic positions were significantly displaced from the ideal bcc lattice positions in the β-type Ti-Mo alloys. In this case, it was difficult to reproduce the density of states (DOS) using the CPA method. The DOS of β, α, and ω Ti–Mo alloys obtained using the CPA method was reported by Cao et al. [19]. While the pseudogaps were near the Fermi level for the α and ω phases, the high DOS peak was located at the Fermi level for the β phase. Therefore, stabilization of the β phase by the addition of Mo atoms was not observed in the DOS obtained using CPA. Fig. 5 shows the DOS of β-type Ti-Mo alloys with and without structural relaxation, obtained using the SQS method. In the DOS of the β-type Ti-Mo alloys without structural relaxations, while the peak at approximately 1 eV decreased with increasing Mo concentration, the positions of the peaks in the valence band were almost unchanged, irrespective of the Mo concentration. However, structural relaxation drastically changed the shape of the DOS around the Fermi level. In the DOS of β-type Ti-Mo alloys with structural relaxations, the peak at approximately 1 eV was shifted downwards by structural relaxations, and a broad pseudogap appeared around the Fermi level. As a result, the Fermi level was located at the bottom of the pseudogap, irrespective of the Mo concentration. These results indicate that structural relaxation plays an important role in stabilizing the bcc structure by the added Mo atoms.

3.4. Vacancy formation and migration energies in Ti-Mo alloy and Ti-15Mo-5Zr-3Al

Fig. 6 shows the average values of the vacancy formation energies of all the sites in the supercell with and without structural relaxation in Ti-14.5Mo (7.8 at%Mo) and Ti-27.0Mo (15.6 at%Mo). The general trend observed was that the energy magnitudes of the Ti and Mo atoms increased with the Mo concentration. The average values without structural relaxation indicate that the Ti atoms possessed higher vacancy formation energies than the Mo atoms. However, the average values with structural relaxation were very similar for the Ti and Mo atoms. This similarity was because of the more significant decrease in energy due to structural relaxation around the Ti vacancies, which arise from the atomic displacement from the ideal bcc lattice positions shown in Fig. 3. In high-entropy alloys (HEA), atomic positrons are displaced from the ideal lattice position because of the difference in the atomic radii of the constituent elements. In a representative HEA, CrMnFeCoNi, the decrease in vacancy formation energies by structural relaxations is approximately 0.5 eV [44]. Therefore, the decrease in energy of more than 1 eV observed in β-type Ti-Mo alloys was a very large energy gain by the structural relaxation. Although the addition of Mo increased the vacancy formation energy by stabilizing the bcc structure, the vacancy formation energies of the Ti and Mo atoms in Ti-14.5Mo and Ti-27.0Mo were still lower than the 1.99 eV vacancy formation energy of α-Ti.

Fig. 7 shows the vacancy formation energies of all sites in the supercell of Ti-15Mo-5Zr-3Al. The average value of each element with and without structural relaxation is represented by cross symbols. The decrease in vacancy formation energies by structural relaxations is more than 1 eV for all the species of the vacancies. The average value with structural relaxations of the Ti vacancies in Ti-15Mo-5Zr-3Al is approximately 0.15 eV higher than that in Ti-14.5Mo, which mainly arises from the decrease in energy gain by the structural relaxation.

To evaluate the effect of Mo atoms on vacancy formation energy, we examined the relationship between the number of Mo atoms around a Ti vacancy and its formation energy. Fig. 8 shows the vacancy formation energies of the Ti atoms in Ti-14.5Mo (7.8 at%Mo) and Ti-27.0Mo (15.6 at%Mo) as a function of the number of neighboring Mo atoms. The vacancy formation energies of the Ti atoms exhibited an increasing trend with an increasing number of neighboring Mo atoms, which suggests that the Mo atoms significantly stabilize neighboring Ti atoms.

To obtain the migration energy of Ti atom in Ti-14.5Mo, we calculated the energy profiles of migration path of the Ti atom exhibiting the vacancy formation energy close to the average value of 0.86 eV using the nudge elastic band method [45,46]. Fig. 9 shows the energy profiles of the migration path of the Ti atom to the eight nearest-neighbor sites. The vacancy formation energies of neighboring Ti sites are widely distributed, from 0.30 to 1.53 eV, which led to the various types of energy profiles of migration paths. The atomic arrangements around the

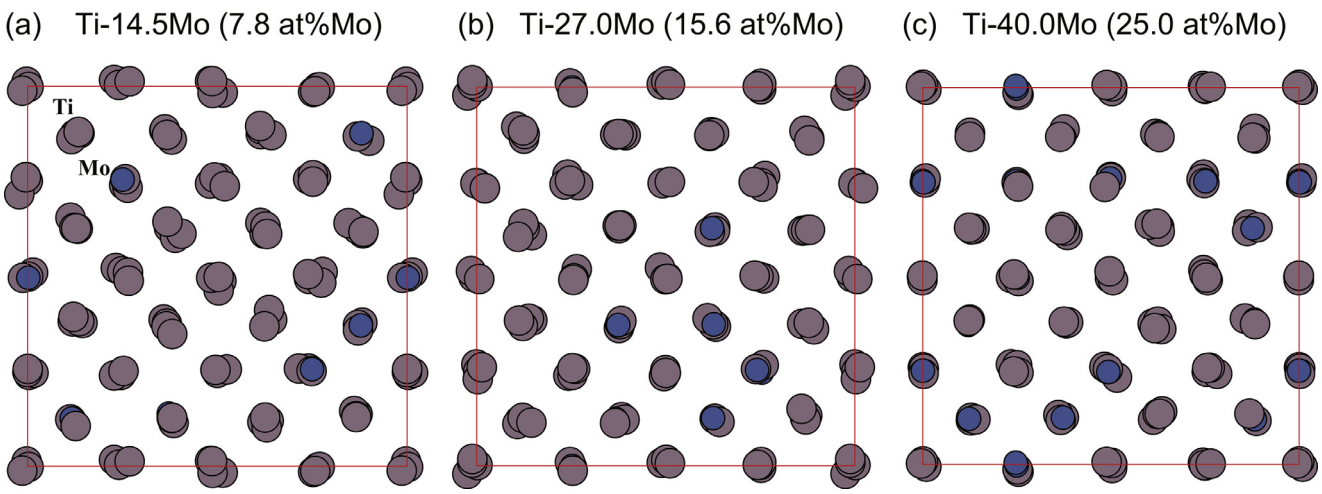

Fig. 4. Atomic arrangement in (a) Ti-14.5Mo (7.8 at%Mo), (b) Ti-27.0Mo (15.6 at%Mo), and (c) Ti-40.0Mo (25.0 at%Mo). Ti and Mo atoms are gray and blue spheres, respectively.

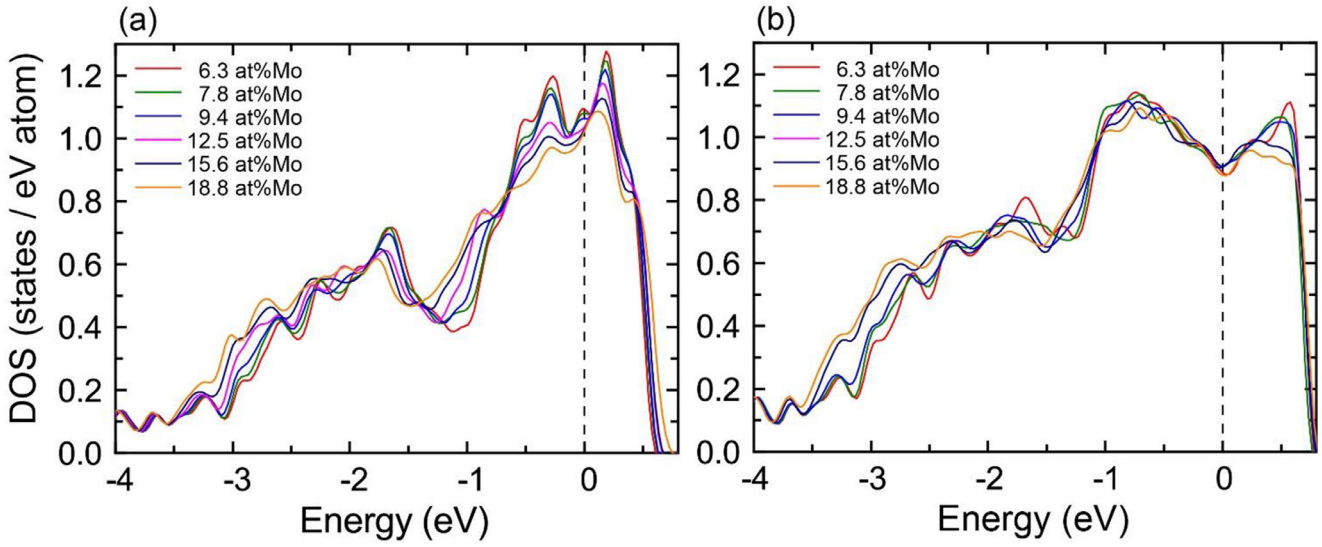

Fig. 5. Total DOS of Ti-Mo alloys (a) without or (b) with structural relaxation.

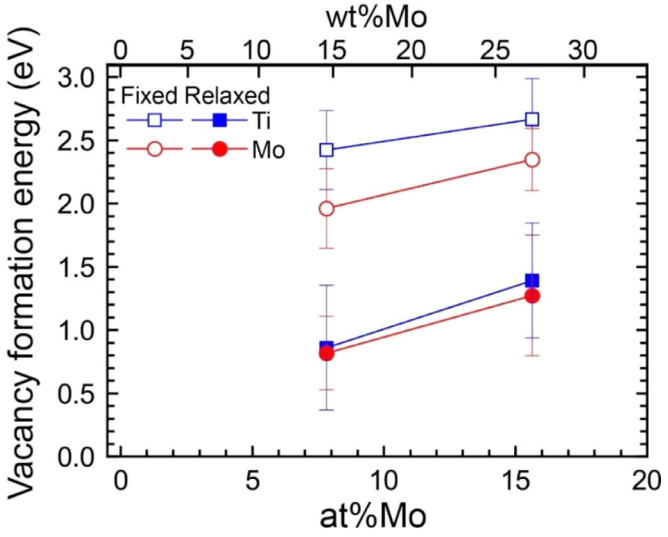

Fig. 6. Average values of vacancy formation energies for Ti and Mo atoms in Ti-14.5Mo (7.8 at%Mo) and Ti-27.0Mo (15.6 at%Mo), with or without structural relaxation.

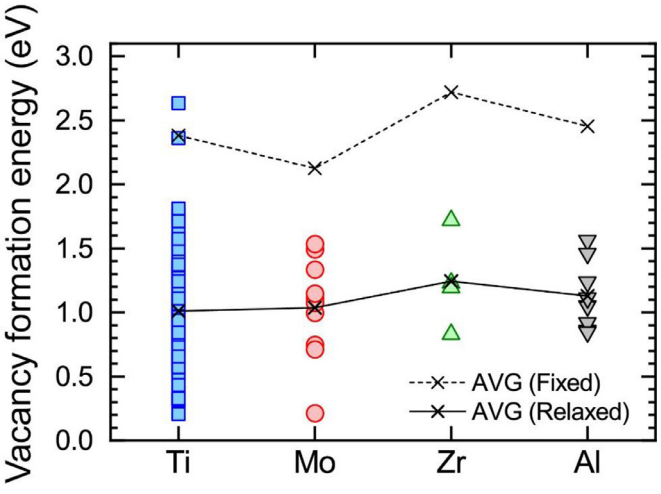

Fig. 7. Vacancy formation energies of all sites in the supercell of Ti-15Zr-5Mo-3Al. Cross symbols denote the average values for each element with or without structural relaxation.

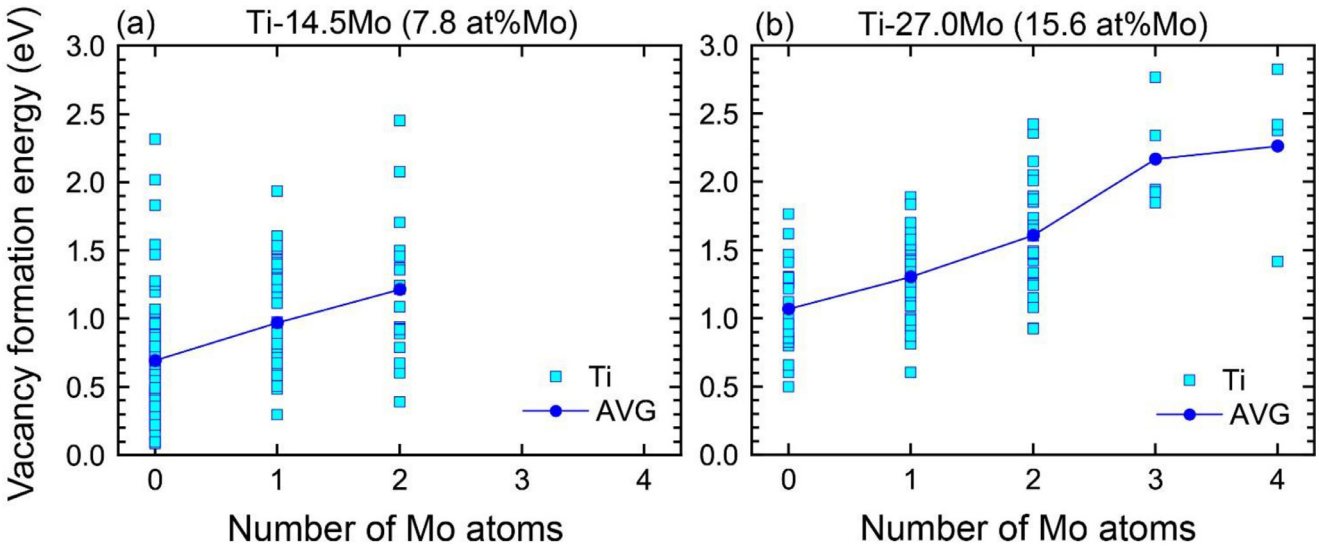

Fig. 8. Vacancy formation energies of Ti atoms in (a) Ti-14.5Mo (7.8 at%Mo) and (b) Ti-27.0Mo (15.6 at%Mo) as a function of the number of neighboring Mo atoms.

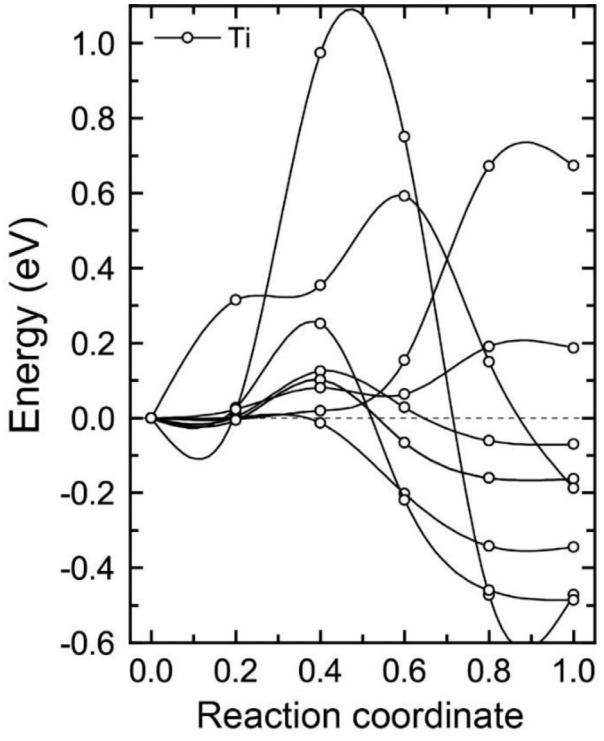

Fig. 9. Energy profiles for migration of the Ti atom to a neighboring vacancy exhibiting the vacancy formation energy close to the average value of 0.86 eV in Ti-14.5Mo.

migration paths and the migration energies are shown in Fig. 10. The migration paths between the Ti sites, surrounded by only Ti atoms, exhibited very low migration energies, ranging from 0.01 to 0.26 eV. On the other hand, the migration paths surrounded by two Mo atoms exhibited higher migration energies than the other migration paths. Therefore, the addition of Mo atoms increases, not only the formation energy, but also the migration energy.

The energy profiles of migration path of the Ti atom in Ti-15Zr-5Mo-3Al was also calculated as shown in Fig.11. We selected four Ti atoms exhibiting the vacancy formation energy close to the average value of 1.01 eV and calculated the energy profiles of the migration path of these Ti atoms to the nearest-neighbor sites. The migration energies are obtained both for the forward and backward directions based on the maximum value of the energy profiles. The average of the migration and formation energies for migration paths shown in Fig. 11 are 0.322 and 0.994 eV, respectively. Compared with 0.274 and 1.06 eV calculated in bcc Ti [30], whereas the bcc structure is stabilized by the addition of Mo atoms, the migration and formation energies are still low enough for diffusion of vacancies, which promoted the annihilation of quenched-in vacancies. Therefore, quenched-in vacancies could be introduced in the other LPBF materials because of the fast cooling rate. In the case of stainless steel 316L, the formation of vacancy-type defects was confirmed by positron lifetime measurements in the LPB specimens build with 370 W laser power and 1350 mm/s scanning speed [47,48].

4. Conclusions

Positron lifetime measurements were performed to identify the lattice defects formed in the LPBF-manufactured β-type Ti-15Mo-5Zr-3Al. Irrespective of the scanning speed, the observed positron lifetimes were close to the experimental and calculated positron bulk lifetimes. Therefore, it has been confirmed that quenched-in vacancies are not introduced in the LPBF-manufactured β-type Ti-15Mo-5Zr-3Al despite the fast cooling rate in LPBF process, which is a preferable feature for the structural stability in biomedical and industrial applications.

To evaluate the effect of Mo atoms on the stability of vacancies, first-principles calculations were performed for the Ti-Mo alloys and Ti-15Mo-5Zr-3Al using the SQS method. The atomic displacement from the ideal bcc lattice positions decreased with increased Mo concentration, indicating that the bcc structure was stabilized by the added Mo. The effect of Mo was also observed in the DOS around the Fermi level, where a broad pseudogap appeared due to structural relaxations. The average vacancy formation energies of Ti and Mo atoms in Ti-Mo alloys increased with increasing Mo concentration. In particular, Mo increased the vacancy formation energies of the neighboring Ti atoms. The migration paths of the vacancies near the Mo atoms exhibited higher migration energies. The calculated results for Ti-15Mo-5Zr-3Al suggest that the migration and formation energies are still sufficiently low for the diffusion of vacancies in β-type Ti-15Mo-5Zr-3Al.

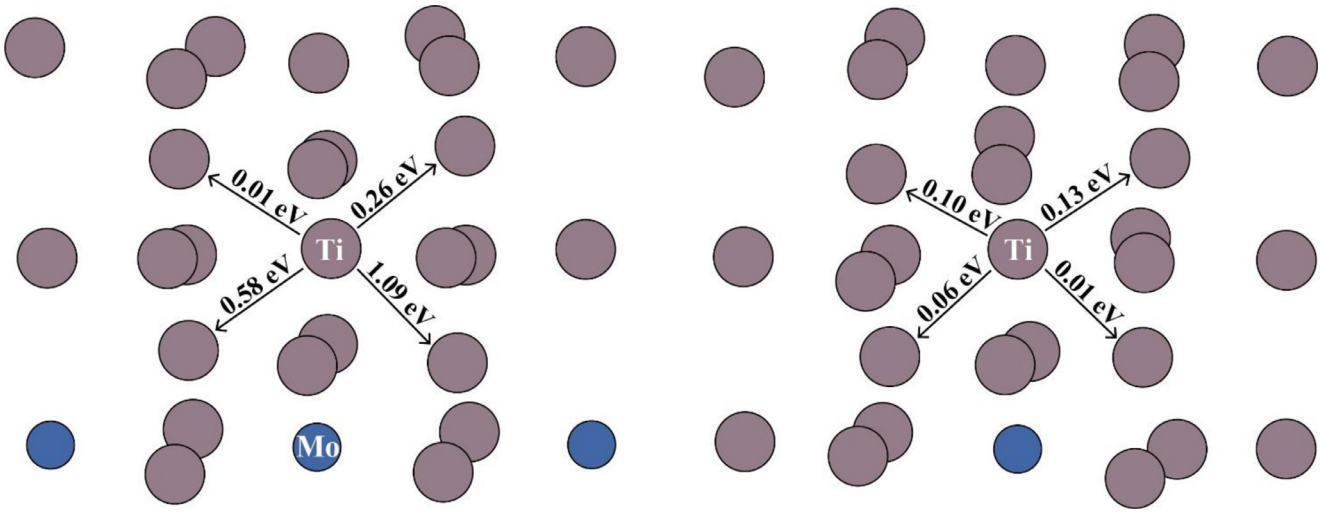

Fig. 10. Atomic arrangement around the migration paths of the Ti atom shown in Fig. 9. Ti and Mo atoms are gray and blue spheres, respectively.

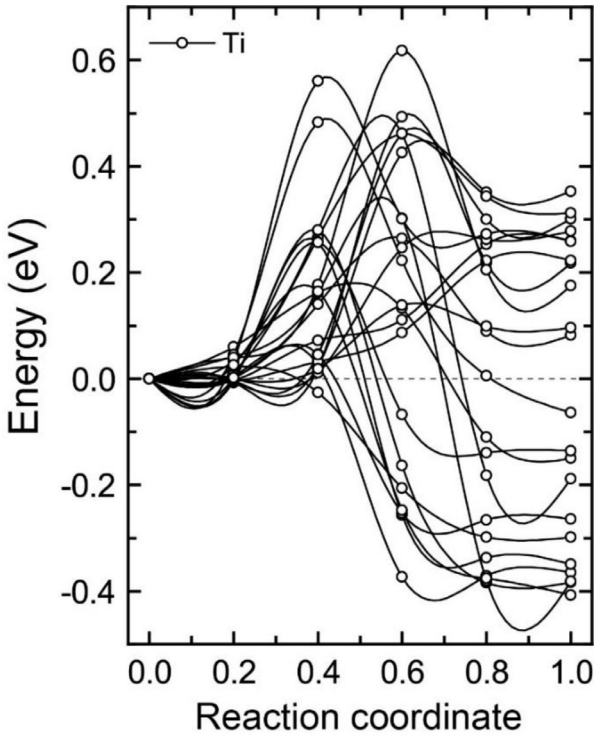

Fig. 11. Energy profiles for migration of the Ti atom to a neighboring vacancy exhibiting the vacancy formation energy close to the average value of 1.01 eV in Ti-15Mo-5Zr-3Al.

Declaration of Competing Interest

The authors declare that they have no known competing financial interests or personal relationships that could have appeared to influence the work reported in this paper.

CRediT authorship contribution statement

Masataka Mizuno: Conceptualization, Methodology, Investigation, Writing – original draft, Writing – review & editing. **Kazuki Sugita:** Investigation, Writing – review & editing. **Kousuke Do:** Investigation, Data curation, Visualization. **Takuya Ishimoto:** Methodology, Validation, Investigation, Data curation, Writing – review & editing. **Takayoshi Nakano:** Conceptualization, Writing – review & editing, Supervision, Project administration, Funding acquisition. **Hideki Araki:** Conceptualization, Writing – review & editing, Supervision, Project administration, Funding acquisition.

Data availability

No data was used for the research described in the article.

Acknowledgment

This work was supported by a Grant-in-Aid for Transformative Research Areas (A) on Creation of Materials by Super Thermal Field: Neo-3D printing by Manipulating Atomic Arrangement through Giant Potential Gradient (Grant number 21H05196) and a Grant-in-Aid for Scientific Research (C) (Grant number 23K04417) from the Japan Society for the Promotion on Science (JSPS). This work was also partially supported by CREST-Nanomechanics: Elucidation of macroscale mechanical properties based on understanding nanoscale dynamics for innovative mechanical materials (Grant Number: JPMJCR2194) from the Japan Science and Technology Agency (JST).

References

[1] M. Niinomi, M. Nakai, J. Hieda, Development of new metallic alloys for biomedical applications, Acta Biomater. 8 (2012) 3888–3903, doi:10.1016/j.actbio.2012.06.037.
[2] L.Y. Chen, Y.W. Cui, L.C. Zhang, Recent development in beta titanium alloys for biomedical applications, Metals 10 (2020) 1139, doi:10.3390/met10091139.
[3] S.S. Sidhu, H. Singh, M.A.H. Gepreel, A review on alloy design, biological response, and strengthening of β-titanium alloys as biomaterials, Mater. Sci. Eng. C 121 (2021) 111661, doi:10.1016/j.msec.2020.111661.
[4] T. Nakano, K. Hagihara, Additive manufacturing of medical devices, in: ASM Handbook, Vol. 23A–Additive Manufacturing in Biomedical Applications, ASM International, Materials Park, OH, 2022, pp. 416–433, doi:10.31399/asm.hb.v23A.a0006905.
[5] P.R. Boyer, G. Welsh, E.W. Collings, Materials Properties Handbook: Titanium Alloys, ASM International, Materials Park, OH, 1994.
[6] S.H. Lee, M. Todai, M. Tane, K. Hagihara, H. Nakajima, T. Nakano, Biocompatible low Young's modulus achieved by strong crystallographic elastic anisotropy in Ti–15Mo–5Zr–3Al alloy single crystal, J. Mech. Behav. Biomed. Mater. 14 (2012) 48–54, doi:10.1016/j.jmbbm.2012.05.005.
[7] M. Tane, K. Hagihara, M. Ueda, T. Nakano, Y. Okuda, Elastic-modulus enhancement during room-temperature aging and its suppression in metastable Ti–Nb-based alloys with low body-centered cubic phase stability, Acta Mater. 102 (2016) 373–384, doi:10.1016/j.actamat.2015.09.030.
[8] K. Hagihara, T. Nakano, Control of anisotropic crystallographic texture in powder bed fusion additive manufacturing of metals and ceramics—A review, JOM 74 (2022) 1760–1773, doi:10.1007/s11837-021-04966-7.
[9] T. Ishimoto, K. Hagihara, K. Hisamoto, S-H. Sun, T. Nakano, Crystallographic texture control of beta-type Ti–15Mo–5Zr–3Al alloy by selective laser melting for the devel-

opment of novel implants with a biocompatible low Young's modulus, Scr. Mater. 132 (2017) 34–38, doi:10.1016/j.scriptamat.2016.12.038.
[10] T. Ishimoto, K. Hagihara, K. Hisamoto, T. Nakano, Stability of crystallographic texture in laser powder bed fusion: Understanding the competition of crystal growth using a single crystalline seed, Addit. Manuf. 43 (2021) 102004, doi:10.1016/j.addma.2021.102004.
[11] S.H. Sun, K. Hagihara, T. Ishimoto, R. Suganuma, Y.F. Xue, T. Nakano, Comparison of microstructure, crystallographic texture, and mechanical properties in Ti–15Mo–5Zr–3Al alloys fabricated via electron and laser beam powder bed fusion technologies, Addit. Manuf. 47 (2021) 102329, doi:10.1016/j.addma.2021.102329.
[12] D. Herzog, V. Seyda, E. Wycisk, C. Emmelmann, Additive manufacturing of metals, Acta Mater. 117 (2016) 371–392, doi:10.1016/j.actamat.2016.07.019.
[13] Q. Jia, P. Rometsch, P. Kürnsteiner, Q. Chao, A. Huang, M. Weyland, L. Bourgeois, X. Wu, Selective laser melting of a high strength: Al–Mn–Sc alloy: alloy design and strengthening mechanisms, Acta Mater. 171 (2019) 108–118, doi:10.1016/j.actamat.2019.04.014.
[14] D. Gu, Q. Shi, K. Lin, L. Xi, Microstructure and performance evolution and underlying thermal mechanisms of Ni-based parts fabricated by selective laser melting, Addit. Manuf. 22 (2018) 265–278, doi:10.1016/j.addma.2018.05.019.
[15] C. Herzig, U. Kohler, Anomalous self-diffusion in BCC IVB metals and alloys, Mater. Sci. Forum 15-18 (1987) 301–322, doi:10.4028/www.scientific.net/MSF.15-18.301.
[16] G. Vogl, W. Petry, Th. Flottmann, A. Heiming, Direct determination of the self-diffusion mechanism in BCC β-titanium, Phys. Rev. B 39 (1989) 5025–5034, doi:10.1103/physrevb.39.5025.
[17] R. Sahara, S. Emura, S. Ii, S. Ueda, K. Tsuchiya, First-principles study of electronic structures and stability of body-centered cubic Ti–Mo alloys by special quasirandom structures, Sci. Technol. Adv. Mater. 15 (2014) 035014, doi:10.1088/1468-6996/15/3/035014.
[18] S. Barzilai, C. Toher, S. Curtarolo, O. Levy, Molybdenum-titanium phase diagram evaluated from ab initio calculations, Phys. Rev. Mater. 1 (2017) 023604, doi:10.1103/PhysRevMaterials.1.023604.
[19] P. Cao, F. Tian, Y. Wang, Effect of Mo on the phase stability and elastic mechanical properties of Ti–Mo random alloys from ab initio calculations, J. Phys. Condens. Matter 29 (2017) 435703, doi:10.1088/1361-648X/aa87d3.
[20] J.L. Zhu, S. Cao, Y. Wang, R. Yang, Q.Mi. Hu, First-principles investigations of ω variant selection during a thermal $\beta \rightarrow \omega$ transformation of binary Ti-xMo alloy, Comput. Mater. Sci. 155 (2018) 524–533, doi:10.1016/j.commatsci.2018.09.028.
[21] F. Jiang, C. Pang, Z. Zheng, Q. Wang, J. Zhao, C. Dong, First-principles calculations for stable β-Ti–Mo alloys using cluster-plus-glue-atom model, Acta Metall. Sin. 33 (2020) 968–974 (Engl. Lett.), doi:10.1007/s40195-020-01006-2.
[22] M. Li, X. Min, Origin of ω-phase formation in metastable β-type Ti-Mo alloys: cluster structure and stacking fault, Sci. Rep. 10 (2020) 8664, doi:10.1038/s41598-020-65254-z.
[23] Q.M. Hu, R. Yang, Unconventional non-uniform local lattice distortion in dilute Ti-Mo solid solution, Acta Mater. 197 (2020) 91–96, doi:10.1016/j.actamat.2020.07.033.
[24] R. Salloom1, S.A. Mantri, R. Banerjee, S.G. Srinivasan, First principles computation of composition dependent elastic constants of omega in titanium alloys: implications on mechanical behavior, Sci. Rep. 11 (2021) 12005, doi:10.1038/s41598-021-91594-5.
[25] Q.J. Chen, S.Y. Ma, S.Q. Wang, The assisting and stabilizing role played by ω phase during the $\{112\}\ <111>_{\beta}$ twinning in Ti-Mo alloys: a first-principles insight, J. Mater. Sci. Technol. 80 (2021) 163–170, doi:10.1016/j.jmst.2020.11.056.
[26] L. Bellaiche, D. Vanderbilt, Virtual crystal approximation revisited: application to dielectric and piezoelectric properties of perovskites, Phys. Rev. B 61 (2000) 7877–7882, doi:10.1103/PhysRevB.61.7877.
[27] N.J. Rammer, A.M. Rappe, Virtual-crystal approximation that works: Locating a compositional phase boundary in $Pb(Zr_{1-x}Ti_x)O_3$, Phys. Rev. B 62 (2000) R743–R746, doi:10.1103/PhysRevB.62.R743.
[28] P. Soven, Coherent-potential model of substitutional disordered alloys, Phys. Rev. 156 (1967) 809–813, doi:10.1103/PhysRev.156.809.
[29] B.L. Gyorffy, Coherent-potential approximation for a nonoverlapping-muffin-tin-potential model of random substitutional alloys, Phys. Rev. B 5 (1972) 2382–2384, doi:10.1103/PhysRevB.5.2382.
[30] S. Kadkhodaei, A. Davariashtiyan, Phonon-assisted diffusion in bcc phase of titanium and zirconium from first principles, Phys. Rev. Mater. 4 (2020) 043802, doi:10.1103/PhysRevMaterials.4.043802.
[31] A. Zunger, S.H. Wei, L.G. Ferreira, J.E. Bernard, Special quasirandom structures, Phys. Rev. Lett. 65 (1990) 353–356, doi:10.1103/PhysRevLett.65.353.
[32] P. Kirkegaard, M. Eldrup, O.E. Mogensen, N.J. Pedersen, Program system for analysing positron lifetime spectra and angular correlation curves, Comput. Phys. Commun. 23 (1981) 307–335, doi:10.1016/0010-4655(81)90006-0.
[33] P. Kirkegaard, M. Eldrup, Positronfit extended: a new version of a program for analysing position lifetime spectra, Comput. Phys. Commun. 7 (1974) 401–409, doi:10.1016/0010-4655(74)90070-8.
[34] X. Gonze, B. Amadon, P.M. Anglade, J.M. Beuken, F. Bottin, P. Boulanger, F. Bruneval, D. Caliste, R. Caracas, M. Côté, T. Deutsch, L. Genovese, Ph. Ghosez, M. Giantomassi, S. Goedecker, D.R. Hamann, P. Hermet, F. Jollet, G. Jomard, S. Leroux, M. Mancini, S. Mazevet, M.J.T. Oliveira, G. Onida, Y. Pouillon, T. Rangel, G.M. Rignanese, D. Sangalli, R. Shaltaf, M. Torrent, M.J. Verstraete, G. Zerah, J.W. Zwanziger, ABINIT: First-principles approach to material and nanosystem properties, Comput. Phys. Commun. 180 (2009) 2582–2615, doi:10.1016/j.cpc.2009.07.007.
[35] E. Boroński, R.M. Nieminen, Electron-positron density-functional theory, Phys. Rev. B 34 (1986) 3820–3831, doi:10.1103/PhysRevB.34.3820.
[36] G. Kresse, J. Hafner, Ab initio molecular dynamics for liquid metals, Phys. Rev. B 47 (1993) 558–561, doi:10.1103/PhysRevB.47.558.
[37] G. Kresse, J. Furthmüller, Efficient iterative schemes for ab initio total-energy calculations using a plane-wave basis set, Phys. Rev. B 54 (1996) 11169–11186, doi:10.1103/PhysRevB.54.11169.
[38] J.P. Perdew, K. Burke, M. Ernzerhof, Generalized gradient approximation made simple, Phys. Rev. Lett. 77 (1996) 3865–3868, doi:10.1103/PhysRevLett.77.3865.
[39] P.E. Blöchl, Projector augmented-wave method, Phys. Rev. B 50 (1994) 17953–17979, doi:10.1103/PhysRevB.50.17953.
[40] G. Kresse, D. Joubert, From ultrasoft pseudopotentials to the projector augmented-wave method, Phys. Rev. B 59 (1999) 1758–1775, doi:10.1103/PhysRevB.59.1758.
[41] J. Cowley, An approximate theory of order in alloys, Phys. Rev. 77 (1950) 669–675, doi:10.1103/PhysRev.77.669.
[42] M.J. Puska, T. Korhonen, R.M. Nieminen, A.P. Seitsonen, Two-component density-functional calculations for positrons trapped by defects in solids, Appl. Surf. Sci. 116 (1997) 293 -229, doi:10.1016/S0169-4332(96)01072-0.
[43] A. Takase, T. Ishimoto, R. Suganuma, T. Nakano, Lattice distortion in selective laser melting (SLM)-manufactured unstable β-type Ti-15Mo-5Zr-3Al alloy analyzed by high-precision X-ray diffractometry, Scr. Mater. 201 (2021) 113953, doi:10.1016/j.scriptamat.2021.113953.
[44] M. Mizuno, K. Sugita, H. Araki, Defect energetics for diffusion in CrMnFeCoNi high-entropy alloy from first-principles calculations, Comput. Mater. Sci. 170 (2019) 109163, doi:10.1016/j.commatsci.2019.109163.
[45] H. Jónsson, G. Mills, K.W. Jacobsen, B.J. Berne, G. Ciccotti, D.F. Coker, in: Classical and Quantum Dynamics in Condensed Phase Simulations–Nudged Elastic Band Method for Finding Minimum Energy Paths of Transitions, World Scientific, Singapore, 1998, pp. 385–404, doi:10.1142/9789812839664_0016.
[46] G. Mills, H. Jonsson, G.K. Schenter, Reversible work transition state theory: application to dissociative adsorption of hydrogen, Surf. Sci. 324 (1995) 305–337, doi:10.1016/0039-6028(94)00731-4.
[47] T.S. Byun, B.E. Garrison, M.R. McAlister, X. Chen, M.N. Gussev, T.G. Lach, A.Le Coq, K. Linton, C.B. Joslin, J.K. Carver, F.A. List, R.R. Dehoff, K.A. Terrani, Mechanical behavior of additively manufactured and wrought 316L stainless steels before and after neutron irradiation, J. Nucl. Mater. 548 (2021) 152849, doi:10.1016/j.jnucmat.2021.152849.
[48] X. Hu, T.G. Lach, K.A. Terrani, Deuterium permeation and retention in 316L stainless steel manufactured by laser powder bed fusion, J. Nucl. Mater. 548 (2021) 152871, doi:10.1016/j.jnucmat.2021.152871.